

Cite this: DOI: 00.0000/xxxxxxxxxx

## Artificial stabilization of the fusion pore by intra-organelle styrene-maleic acid copolymers<sup>†</sup>

Marcelo Caparotta,<sup>a</sup> Marcelo Puiatti,<sup>b</sup> and Diego Masone<sup>\*,c,d</sup>Received Date  
Accepted Date

DOI: 00.0000/xxxxxxxxxx

Styrene-maleic acid copolymers have become an advantageous detergent-free alternative for membrane protein isolation. Since their discovery, experimental membrane protein extraction and purification by keeping intact their lipid environment has become significantly easier. With the aim of identifying new applications of these interesting copolymers, their molecular binding and functioning mechanisms have recently been intense objects of study. In this work, we describe the use of styrene-maleic acid copolymers as an artificial tool to stabilize the fusion pore. We show that when these copolymers circumscribe the water channel that defines the fusion pore, they keep it from shrinking and closing. We describe how only intra-organelle copolymers have stabilizing capabilities while extra-organelle ones have negligible or even contrary effects on the fusion pore life-time.

### 1 Introduction

Exocytosis is a fundamental process used by eukaryotic cells to release biological compounds and to insert lipids and proteins in the plasma membrane. Specialized secretory cells undergo regulated exocytosis in response to physiological signals<sup>1–3</sup>. In particular, sperm exocytosis or acrosome reaction is a regulated secretion with special features required to fertilize the egg, one such feature is extensive membrane remodelling, including membrane bending and fusion<sup>2,4–6</sup>.

In this remarkable process multiple fusion pores open between the outer acrosomal membrane and the overlying plasma membrane, connecting the lumen of the acrosome to the extracellular milieu. Therefore, the fusion pore functions as an effective mechanism to connect intracellular organelles and release vesicle

contents during exocytosis. Although the nucleation of the fusion pore is thermodynamically unfavourable (and thought to be mediated by specialized proteins), it is widely accepted that once formed the pore can evolve following different paths: rapid dilation, slow expansion, transient flickering (open-close repetitions) and also resealing<sup>6</sup>.

The stabilization of the fusion pore by specialized proteins has been extensively studied experimentally<sup>7–10</sup> and computationally<sup>5,11,12</sup> being a fundamental molecular mechanism relevant for the understanding of the diverse roles of the cellular fusion machinery<sup>12</sup>. The prospect of a rational mechanism to stabilize the fusion pore has implications in exocytosis control, vesicle content discharge regulation, fusion pore gating and diameter regulation<sup>7</sup>.

An interesting approach from synthetic biology is the production of complex synthetic organisms that perform useful functions<sup>13</sup>. The use of artificial molecules to mimic or to interfere with cellular properties and behaviours has helped to understand the working mechanisms of a cell<sup>14</sup>. In particular, styrene-maleic acid copolymers (SMACs) have shown remarkable capabilities to effectively solubilize biological membranes into nanodiscs, allowing for simpler protein isolation directly from their native environment without the use of detergents<sup>15,16</sup>. Therefore, they have become an interesting tool for the study and characterization of membrane proteins<sup>17–19</sup> with already promising results<sup>20–23</sup>.

Inspired by the natural protein-mediated processes known for fusion pore stabilization<sup>7,8,10,24,25</sup>, we describe here an artificial alternative. We show that SMACs have the ability to stabilize the fusion pore in terms of its life-time. When located inside the organelles connected by the fusion pore (above and below the bilayers) SMACs bind to the membranes, diffuse towards the water channel and prevent the fusion pore from collapsing. Remark-

<sup>a</sup> Facultad de Ciencias Exactas y Naturales, Universidad Nacional de Cuyo (UNCuyo), 5500, Mendoza, Argentina

<sup>b</sup> Instituto de Investigaciones en Físico-Química de Córdoba (INFIQC) - Consejo Nacional de Investigaciones Científicas y Técnicas (CONICET), Universidad Nacional de Córdoba (UNC), 5016, Córdoba, Argentina

<sup>c</sup> Facultad de Ingeniería, Universidad Nacional de Cuyo (UNCuyo), 5500, Mendoza, Argentina

<sup>d</sup> Instituto de Histología y Embriología de Mendoza (IHEM) - Consejo Nacional de Investigaciones Científicas y Técnicas (CONICET), Universidad Nacional de Cuyo (UNCuyo), 5500, Mendoza, Argentina, Tel: +54 261 405 4843; E-mail: diego.masone@ingenieria.uncuyo.edu.ar

<sup>†</sup> Electronic Supplementary Information (ESI) available: simulation repetitions; minimum distance measurements from nearest SMACs to the centre of the fusion pore; correlation between lipid mean squared displacements and SMAC:lipid contacts; plot averaged SMAC:lipid contacts per lipid species; correlation between radius of gyration and SMAC:lipid contacts; measurement of SMAC self-interactions; plots of density charge profiles along Z axis while the fusion pore is open; second-rank order parameter calculations along with tables S1, S2 and S3 listing bonds between beads; table S4 listing details of all simulations performed in this study. See DOI: 00.0000/00000000.

ably, the stabilization of the fusion pore is mainly dependent on the amount of intra-organelle SMAC:lipid contacts, with no significant intervention from extra-organelle SMACs (located in the cytosolic water, between the bilayers, see figure 1).

## 2 Results and Discussion

We have conducted unbiased molecular dynamics simulations for SMACs located between and above/below the bilayers belonging to two different organelles (see figure 1a). In this arrangement the intra and extra-organelle spaces are mutually exclusive (see inset in figure 1a) and do not share molecules neither before nor after the fusion pore has been formed (see figure 1b). We have induced the formation of the fusion pore from initially flat and parallel bilayers using our in-house collective variable procedure<sup>5</sup>. For SMACs in the MARTINI coarse-grained space<sup>26</sup> we have used the parameters developed by Prof. Orekhov (who generously shared his files with us through personal communications) to study lipid patches in the bilayer<sup>27</sup>, see figure 2.

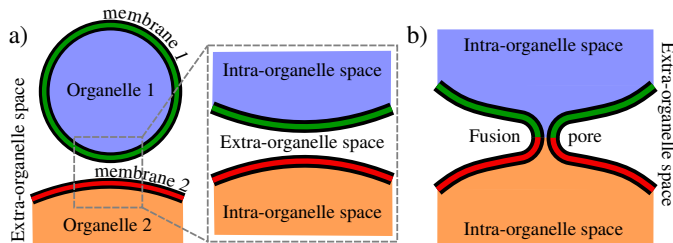


**Fig. 1 Independent organelles nucleating a fusion pore.** a) Organelles about to fuse. Intra-organelle contents are colored in violet and orange, white is left for the extra-organelle environment. b) Organelles connected by a fusion pore.

We have used biologically relevant membranes including 1-palmitoyl-2-oleoyl-glycero-3-phosphocholine (POPC), 1-palmitoyl-2-oleoyl-sn-glycero-3-phospho-L-serine (POPS) and the MARTINI POP2 general model for phosphatidylinositol bisphosphate lipids, corresponding to the atomistic model C16:1(9c),C18:1(9c) dioleoyl (DO-PIP<sub>2</sub>)<sup>26,28–30</sup>. This ternary membrane composition (POPC:POPS:POP2) is analogous to the plasma membrane used experimentally by Jahn and collaborators<sup>31</sup> to trap synaptotagmin-1 to the plasma membrane in the presence of calcium.

### 2.1 Intra-organelle SMACs stabilize the fusion pore

As observed by Marrink and collaborators<sup>32</sup>, SMACs bind to the membrane generally during the first few nanoseconds of the simulation due to the high SMAC-membrane affinity. Under the fusion pore configuration, we have observed that intra-organelle SMACs stabilize the pore, preventing its traversing water channel to collapse and the bilayers to detach.

We have determined fusion pore closure time by dynamically counting the amount of C4 tail lipid beads present in the space between the lipid bilayers (see figure 3a). For planar and parallel membranes there are no C4 beads between the bilayers simply because all lipid tails point toward their respective bilayer interiors. On the other hand, for the formed fusion pore (where lipids surrounding the water channel are gradually tilted toward the

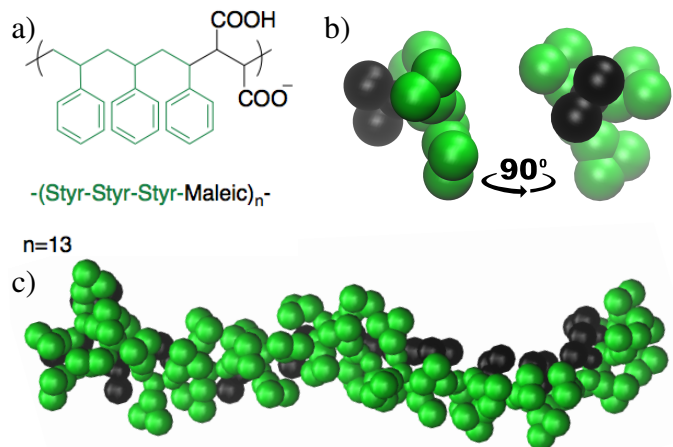


**Fig. 2 Styrene-maleic acid copolymers.** a) Structural formula of an SMA copolymer. b) Beads representation of a 3:1 Styrene/Maleic ratio SMAC fragment. Side and front views. c) A SMAC containing 195 beads. In all cases, maleic acid beads are black and styrene ones are green.

opposite bilayer describing a clean membrane fusion path), the amount of C4 beads increases as a function of the fusion pore width. For more details on lipid tilting and splaying during membrane fusion see Mirjanian et al.<sup>33</sup> and Caparotta et al.<sup>5</sup>.

To measure effective SMAC:lipid interactions, we have counted the number of bead contacts ( $<0.5$  nm) between both groups (SMAC beads and lipid beads), normalized by the number of SMACs in each simulation (see figure 3c). In cases with poor or low SMAC:lipid interactions, the SMAC-driven stabilization of the fusion pore did not take place and the pore closed (simulations #5 and #6). A snapshot of simulation #5 (figure 3b, left) just before pore closure ( $0.19 \mu\text{s}$ ) suggests insufficient SMA-membrane interactions, unlike the snapshot of simulation #3 (figure 3d, left) at the same time with two SMACs already fully inserted in the membranes, parallel to each lipid-water intra-organelle interface.

Snapshots of these two simulations (#3 and #5) were also taken at  $t=3.5 \mu\text{s}$  showing for simulation #5 (figure 3b, right) a complete recovery of the bilayers after the fusion pore closure. On the other hand, simulation #3 (figure 3d, right) shows a well-stabilized fusion pore with SMACs inside the bilayers and surrounding the water channel.

Simulations #1 to #4 are examples of the intra-organelle SMAC-driven stabilization. On the other hand, simulations #5 and #6 constitute a counterexample, showing that the amount of intra-organelle SMACs is only a necessary condition for fusion pore stabilization, which becomes sufficient when steady SMAC:lipid contacts are able to establish (simulations #1 to #4). Overall, for different amounts of intra-organelle SMACs (4, 8, 12 and 24) the fusion pore is stabilized in terms of its life-time, if and only if effective contacts exist between the SMACs and the lipid bilayers.

Panel 3e is a time extension of panel 3a, showing the amount of C4 beads surrounding the fusion pore until  $t=10 \mu\text{s}$  for simulations #1 to #4. Importantly, simulations #1, #2, #3 (red, blue and green lines) indicate the stabilization of the fusion pore with almost constant values of C4 beads, while for simulation #4 the pore

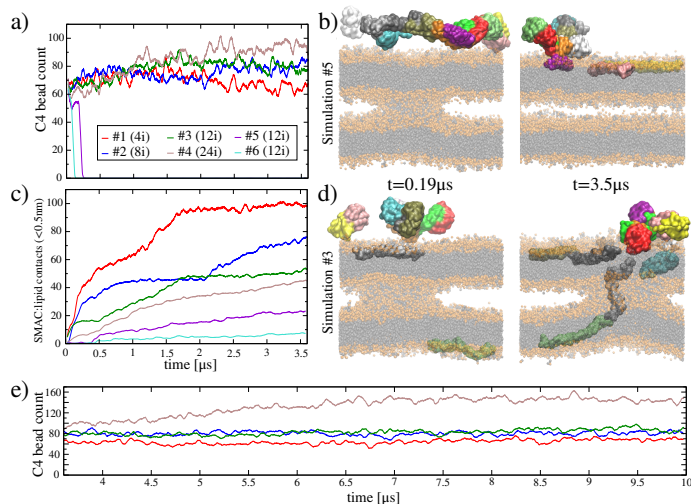


**Fig. 3** Intra-organelle SMACs. **a)** C4 tail bead count between the bilayers. All simulations correspond to intra-organelle (i) SMACs, in different amounts (4, 8, 12 and 24) and for each amount simulations were repeated twice (see supplementary information for repetitions of simulations #1, #2 and #4). **b)** Molecular dynamics snapshots for simulation #5 at two times:  $t=0.19\mu\text{s}$  and  $t=3.5\mu\text{s}$ . **c)** Normalized SMAC:lipid bead contacts ( $<0.5\text{nm}$ ). **d)** Molecular dynamics snapshots for simulation #3 at two times:  $t=0.19\mu\text{s}$  and  $t=3.5\mu\text{s}$ . PO4, GL, NC3 and D2A beads are orange, the rest of lipid beads are grey. Water molecules are not shown. **e)** Extension until  $10\mu\text{s}$  of simulations #1, #2, #3 and #4.

widens significantly (almost doubling the amount of C4 beads surrounding the water channel). This result means that the fusion pore enters in an expansion regime (until  $\approx 6.5\mu\text{s}$ ) before stabilizing at a higher value ( $\approx 150$  C4 beads).

## 2.2 Extra-organelle SMACs have unfavourable stabilization effects

As before, panel 4a shows the amount of C4 beads between the bilayers to measure the time of pore closure, now in the presence of extra-organelle SMACs exclusively. Analogously, figure 4c shows SMAC:lipid contacts ( $<0.5\text{nm}$ ). It can be observed that in all cases (simulations #7 to #12) the fusion pore collapses before  $1.5\mu\text{s}$  while the number of SMAC:lipid contacts keeps increasing (#9 to #12) until saturation (#7 and #8). Interestingly, the steady state regime in panel 4c correlates to the fusion pore closure time. Simulations #7 and #8 (magenta and orange curves) show the fastest increase of SMAC:lipid contacts and are also the first ones where the pore collapses. On the contrary, simulations #9 and #11 (violet and red) are the ones with the largest transient regime in SMAC:lipid amount of contacts terms and the ones with the longest lifespan pores, suggesting that extra-organelle SMAC:lipid contacts have inverse effects in fusion pore stabilization. In all cases studied here, no permanent fusion pore stabilization is achieved by extra-organelle SMACs exclusively.

Figures 4b and 4d correspond to a set of eight simulations (#13 to #20) containing both intra and extra-organelle SMACs in different proportions (the first number between parenthesis is the amount of extra-organelle SMACs followed by the num-

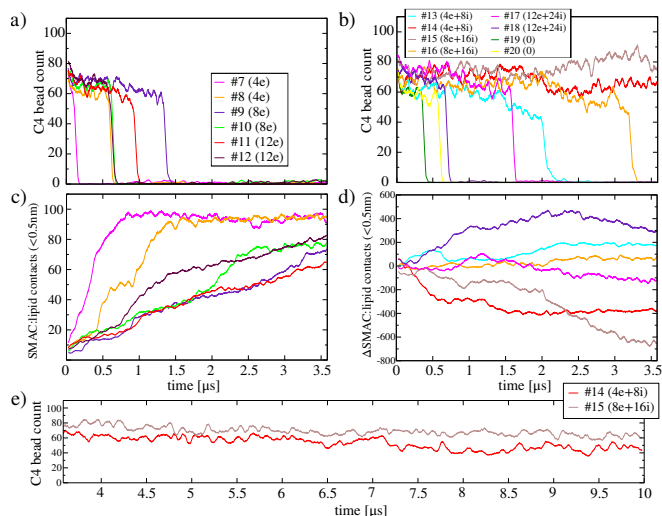


**Fig. 4** Extra-organelle and hybrid extra/intra-organelle SMACs. **a)** and **b)** C4 tail bead count between the bilayers. **c)** Normalized SMAC:lipid bead contacts ( $<0.5\text{nm}$ ). Simulations were repeated once and correspond to extra-organelle (e) SMACs, in different amounts (4, 8 and 12). **d)** Difference ( $\Delta$ ) between extra and intra-organelle normalized SMAC:lipid contacts ( $<0.5\text{nm}$ ). Simulations were repeated once and include different amounts of extra-organelle (e) and intra-organelle (i) SMACs. **e)** Extension until  $10\mu\text{s}$  of simulations #14 (4 extra-organelle and 8 intra-organelle SMACs) and #15 (8 extra-organelle and 16 intra-organelle SMACs).

ber of intra-organelle ones). Panel 4b measures the amount of C4 beads between the bilayers to determine the pore closure time. Panel 4d shows the difference between the extra-organelle SMAC:lipid contacts and the intra-organelle ones. Therefore, curves above zero are simulations with greater amounts of extra-organelle SMAC:lipid contacts and curves with negative values are simulations with relatively larger amounts of intra-organelle SMAC:lipid contacts.

It is observed that the first pores to collapse are those with no SMACs included (#19 green and #20 yellow lines), followed by the one with the highest amount of extra-organelle SMAC:lipid contacts (#18 violet line) which closes at  $\approx 0.75\mu\text{s}$ .

The next pores to close are the next ones in descending order of extra-organelle SMAC:lipid contacts (#17 magenta and #13 cyan) at  $\approx 1.6\mu\text{s}$  and  $\approx 2.1\mu\text{s}$ . Finally, the last pore to close is also the last one in descending order of extra-organelle SMAC:lipid contacts (#16 orange) at  $\approx 3.3\mu\text{s}$ . As expected, simulations reaching negative values in panel 4d, establishing less extra-organelle SMAC:lipid contacts and more intra-organelle ones (#14 red and #15 brown), correspond to the fusion pores that do not close. Panel 4e shows the time extension of simulations #14 to #15 until  $10\mu\text{s}$  to verify the SMAC-driven fusion pore stabilization mechanism. Therefore, permanent intra-organelle SMAC:lipid contacts and their dominance over extra-organelle ones, is a direct measure of the lifespan of the fusion pore.

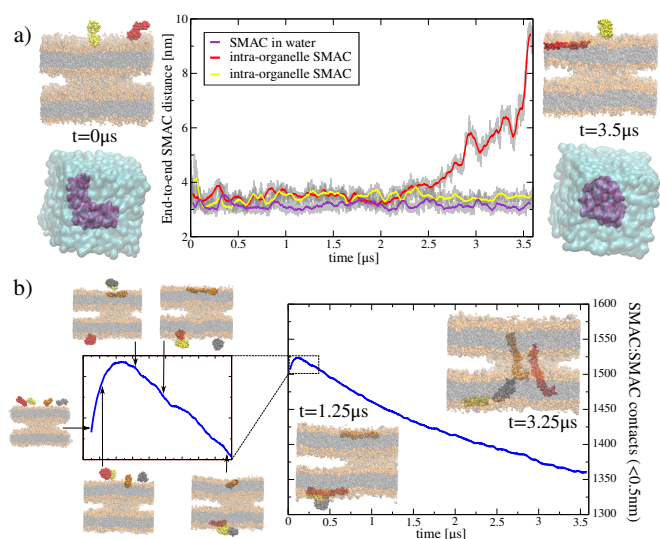


**Fig. 5 SMACs extension and diffusion in the fusion pore.** a) SMACs end-to-end distance over time as they diffuse in the bilayer for two intra-organelle SMACs (yellow and red) and a single SMAC (purple) solvated in water. Line colours match molecule colours. Water molecules are only shown as cyan surface representation for the single SMAC solvated in water without bilayers. b) Averaged SMAC:SMAC amount of self-contacts over time. Inset on the left details the initial behaviour.

### 2.3 SMACs extend and isolate from other SMACs as they migrate into the bilayer

As SMACs diffuse into the bilayers they experiment their own conformational changes. Figure 5a describes the SMACs end-to-end distance as a function of time for different setups: (i) yellow and red lines correspond to yellow and red intra-organelle SMACs as shown in top-left and top-right snapshots at  $t=0$  and  $t=3.5\mu\text{s}$  respectively and (ii) purple line corresponds to a (purple) SMAC solvated in water with no bilayers present. Remarkably, the yellow SMAC that remains outside the bilayers keeps a globular conformation (yellow line) just like the purple SMAC solvated in water without bilayers (purple line). On the other hand, the SMAC that penetrates the membrane (red molecule) and locates itself below the lipid-water interface, extends to its full length  $\approx 9\text{nm}$  (red line) at  $t\approx 3.5\mu\text{s}$ .

To describe how intra-organelle SMACs collectively self-organize to stabilize the fusion pore we have measured the amount of SMAC:SMAC contacts ( $<0.5\text{nm}$ ) over time. Figure 5b shows the time evolution of 4 intra-organelle SMACs initially located above the bilayers (see inset in figure 5b, left snapshot at  $t=0$ ). During the first  $\approx 250\text{ns}$  SMACs transiently bind together but rapidly reduce their mutual interactions which are replaced by SMAC:lipid ones (see inset). For the rest of the time SMAC:SMAC contacts decrease monotonically while the fusion pore is stabilized, see snapshot at  $t\approx 3.25\mu\text{s}$  with 4 SMACs inside the bilayers and 2 SMACs fully inserted in the pore (orange and red), surrounding the water channel. Therefore, as the fusion pore is stabilized SMACs coordinate around the water channel along the perpendicular axis to the bilayers in a fully extended conformation.

### 2.4 SMACs reduce the total mobility of the lipids and the amount of water molecules trapped inside the bilayers

When the fusion pore is fully formed, lipids surrounding the water channel orient themselves radially with their tails towards the centre of the traversing channel (see red lipids in molecular dynamics snapshots in figure 6a). Therefore, the amount of C4 tail beads in transient contact with water molecules (either from intra or extra-organelle spaces) is increased due to the natural toroidal geometry of the fusion pore (although other geometries have been observed<sup>34,35</sup>). When the pore collapses and the bilayers recovery to their planar and parallel configurations, lipid tails return inside the bilayer core and lipids expose their phosphate groups toward the water interfaces. During this complex lipid re-organization<sup>36,37</sup> the amount of C4:water (C4:PW) contacts are a measure of how many water molecules are trapped, on average, inside the bilayers.

Figure 6a shows this count starting from a formed fusion pore without SMACs (cyan line) and for the same system but with 36 SMACs (12 extra-organelle and 24 intra-organelle). The time instant when the pore closes is indicated for both simulations as a step down in the C4 count. Although the closure event marginally reduces C4:water contacts, it is observed that the presence of SMACs reduce the amount of waters inside the bilayer (orange line). Molecular dynamics snapshots in panel 6a show representative splaying lipids (red molecules) and intra-organelle SMACs ascending inside the pore through the water channel (blue molecules).

Nevertheless, we have observed a special case where one extra-organelle SMAC connects both bilayers (in a bridge-like way) which has the opposed effect. Under this particular configuration, a single extra-organelle SMAC mechanically pulls from both bilayers toward the centre of the inter-membrane space, disordering membrane molecules at the lipid-water interface and facilitating the infiltration of water molecules.

The mobility of all lipid molecules is also affected by their interactions with SMAC molecules, particularly, the total lipidic Mean Squared Displacement (MSD) is reduced by increasing amounts of SMAC:lipid contacts (see figure S5 in supplementary information). In the stabilized fusion pore, the amount of SMAC:lipid contacts increases together with the radius of gyration of all SMACs (see figure S7 in supplementary information), while the ensemble average of SMAC self-interactions monotonically decreases over time (see figure S8 in supplementary information). These effects combined support the premise that establishing steady state SMAC:lipid contacts promotes SMACs to isolate and to increase their conformational exploration space.

The distance between the centre of the pore and the nearest intra-organelle SMAC has also shown to be determinant for fusion pore stabilization, during the first hundreds of nanoseconds in conditions with already high amounts of SMAC:lipid contacts (see figures S3 and S4 in supplementary information).

Finally, no significant effects on the second rank order parameter ( $P_2$ , eq. 1) were observed along simulations where the pore was stabilized and where it was not (see figures S10 and S11 in supplementary information), indicating negligible effects on pos-

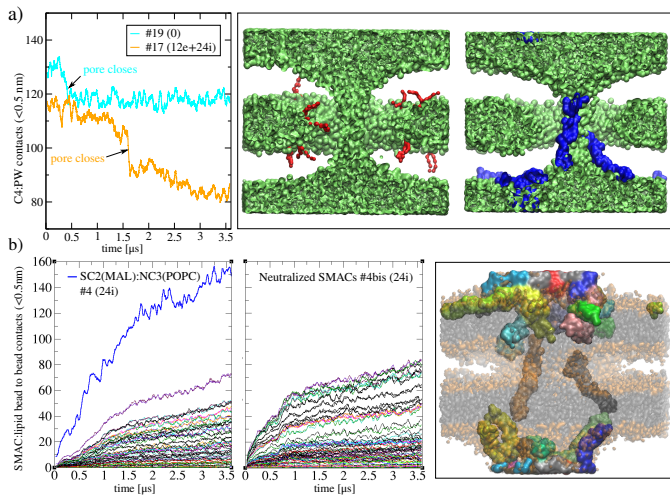


**Fig. 6** a) SMACs reduce the amount of trapped waters inside the bilayer. Curves show lipids tail beads (C4) to water beads (PW) contacts  $< 0.5\text{nm}$  for an initial fusion pore with no SMACs (cyan line) and an identical fusion pore with 36 SMACs (orange line). Arrows indicate the closure time for both unbiased simulations. Molecular dynamics snapshots on the right show water molecules in green with splaying lipids in red and SMACs in blue. b) Neutralized SMACs also stabilize the fusion pore. Left, SMAC:lipid bead-to-bead number of contacts for an unbiased simulation of a fusion pore with 24 intra-organelle SMACs. Middle, an identical arrangement but with neutralized SMACs. Right, molecular dynamics snapshot shows zero-charge SMACs with the stabilized fusion pore. For clarity, water molecules are not shown.

sible phase transitions of the bilayer.  $P_2$  measures the tilting of hydrophobic lipid chains using equation 1,

$$P_2 = \frac{1}{2}(3\cos^2\theta - 1) \quad (1)$$

where  $\theta$  is the angle between the vector defined by the head group to hydrophobic beads and the axis normal to the bilayer. Then,  $P_2=1$  indicates perfect alignment,  $P_2=-0.5$  indicates perpendicular alignment and  $P_2=0$  indicates random alignment. For more details on this parameter see Marrink et al.<sup>30</sup>.

### 2.5 Neutralized intra-organelle SMACs also stabilize the fusion pore

To quantify which SMAC:lipid bead-to-bead interactions are more relevant during the stabilization of the fusion pore, we have measured all pairwise interactions between SMACs beads and lipid beads in an unbiased simulation with 24 intra-organelle SMACs. As observed in panel 6b on the left, the main interactions are the SC2 beads in SMACs maleic acid with NC3 beads in POPC lipids (blue solid line), with more than two times the amount of SMAC:lipid contacts compared to the rest. This dominant SC2:NC3 interaction accounting for the highest amount of steady state contacts is not unexpected as maleic acid SC2 beads (as parametrised by Orekhov et al.<sup>27</sup>) are negatively charged (-1) while NC3 beads in POPC molecules are positively charged (+1), as defined for MARTINI, being NC3 beads in POPC the only lipid bead positively charged for this membrane (POPC:POPS:POP2). For more details see figure S6 in supplementary information.

To determine if SC2:NC3 electrostatic interactions are exclusively responsible for the whole fusion pore stabilization process, we neutralized the -1 charge in all SMACs SC2 beads. By repeating the simulation under identical conditions we obtained the SMAC:lipid bead-to-bead interactions shown in panel 6b on the right, where no significantly dominant bead-to-bead interactions can be distinguished. Surprisingly, the fusion pore is again stable under these conditions (see snapshot inset in panel 6b on the right), suggesting that the whole group of SMAC:lipid interactions are still robust enough to compensate the absence of the main electrostatic interactions and nevertheless extend the life of the pore. Table 1 shows SMAC:lipid bead-to-bead interactions in descending order of importance for both cases: neutralized (SC2=0) and originally charged SMACs (SC2=-1). See figure S9 in supplementary information for density charge profiles along the normal axis to the bilayers.

**Table 1** SMAC:lipid bead-to-bead interactions in descending order of importance in terms of the amount of contacts

position	Neutralized SMACs (SC2=0)	Charged SMACs (SC2=-1)
1	SC2(STY):C1A	SC2(MAL):NC3
2	SC2(STY):C4A	SC3/SC2(STY):C1A
3	SC3(STY):C1A	SC2(STY):D2A
4	SC3(STY):C4A	SC3(STY):D2A

## 3 Conclusions

In this work we have shown how styrene-maleic acid copolymers located in the intra-organelle space function as stabilizers of the fusion pore. We have conducted  $\mu\text{s}$ -length coarse-grained unbiased molecular dynamics to measure the life-time of the fusion pore in the presence of different amounts of SMACs, located in both intra and extra-organelle spaces, exclusively and simultaneously. We have shown that the amount of intra-organelle SMAC:lipid contacts that spontaneously form are the key in the stabilization mechanism, being extra-organelle ones inconsequential or even antagonistic to this end. As stabilized pores are less likely to proceed to the expansion regime<sup>7</sup>, an event facing a major energy barrier<sup>38</sup>, we propose SMACs as an artificial tool to stabilize the fusion pore by tuning its dynamics, to control exocytosis and to regulate vesicle cargo discharge.

## 4 Computational Methods

We have conducted all our simulations with the MARTINI coarse-grained model<sup>26</sup> using SMACs parameters developed by Orekhov et al.<sup>27</sup>. In all cases the bilayers used were POPC:POPS:POP2 in concentrations (85:10:5), constructed with the CHARMM-GUI web server<sup>39</sup>. All bilayers contained 1024 molecules each ( $\approx 17 \times 17 \text{ nm}$ ), which ensures negligible finite-size effects due to interactions between periodic images of the fusion pore<sup>5</sup>. Each bilayer was initially solvated in more than  $\approx 15 \times 10^3$  PW coarse-grained polarizable water molecules<sup>40</sup> to fulfil the ample water condition for MARTINI<sup>29</sup>. When merged together, the amount of extra-organelle water molecules (confined between the bilayers) was adjusted to equilibrate the inter-membrane separation distance at  $\approx 3.5 \text{ nm}$ , in resemblance to the protein-mediated fu-

sion pore stabilization by one synaptotagmin-1 C2B domain<sup>5</sup>. It has been suggested that inter-membrane distance could also be a mechanism to stabilize fusion pores against re-closure<sup>41</sup>. For a detailed description of inter-membrane distances effects, see Smirnova et al.<sup>42</sup>.

Molecular dynamics simulations were performed with GROMACS-2020.2<sup>43–45</sup> with the semi-isotropic NPT ensemble and a time step of 20fs in all cases, with the exception of the simulation of a single SMAC solvated in water (no bilayers) where the isotropic ensemble was used instead. The temperature,  $T=303.15\text{K}$ <sup>46–50</sup>, was controlled by a V-rescale thermostat<sup>51</sup> using a coupling constant of 1ps. The pressure was maintained at 1.0bar and compressibility was set to  $3 \times 10^{-4} \text{bar}^{-1}$ . For equilibration runs the Berendsen barostat<sup>52</sup> was used with a time constant of 5ps while for production the Parrinello-Rahman barostat<sup>53</sup> was used instead, with a time constant of 12ps. Neighbour searching was performed using a Verlet cut-off scheme with a buffer tolerance of 0.005kJ/mol/ps. The minimum frequency to update the neighbour list was set to 20 steps with periodic boundary conditions (PBC) in all directions. The reaction field method was employed for Coulomb interactions with a cut-off of 1.1nm and a relative dielectric constant of 2.5. Van der Waals interactions were treated using the cut-off scheme with a cut-off of 1.1nm. Before production runs, all systems were minimized and equilibrated for at least 100ns to generate properly relaxed initial configurations.

SMAC:lipid and SMAC:SMAC interactions were measured with GROMACS *gmx mindist* implementation using option -group, to count contacts with multiple beads in the first group as one. Molecular dynamics snapshots were visualized using Visual Molecular Dynamics (VMD)<sup>54</sup>. Data graphics were plotted with Grace (GRaphing, Advanced Computation and Exploration of data). Figure panels were organized using Inkscape and GIMP (GNU Image Manipulation Program).

## Author Contributions

DM conceived the idea and supervised the research. DM and MC designed the computational experiments with support from MP. MC performed the numerical simulations. DM wrote the manuscript in consultation with MC and MP. All authors discussed the results and contributed to the final manuscript.

## Conflicts of interest

There are no conflicts to declare.

## Acknowledgements

Supercomputing time for this work was provided by CCAD (Centro de Computación de Alto Desempeño de la Universidad Nacional de Córdoba) and by SNCAD-MinCyT Iniciativa de Proyectos Acelerados de Cálculo (IPAC), grant numbers: 2017-75-APN-SECACT #MCT, 2018-6-APN-SECACT #MECCYT and 2019-72-APN-SECACT#MECCYT. Also, grants from CONICET (PIP-13CO01), ANPCyT (PICT2017-1002) and GPU hardware by the NVIDIA Corporation are gratefully acknowledged. The authors thank Prof. Philipp Orekhov for sharing his molecular model of styrene-maleic acid copolymers for MARTINI.

## Notes and references

- 1 M. F. Quevedo, M. A. Bustos, D. Masone, C. M. Roggero, D. M. Bustos and C. N. Tomes, *Biochimica et Biophysica Acta (BBA) - Molecular Cell Research*, 2019, **1866**, 612–622.
- 2 A. T. Brunger, U. B. Choi, Y. Lai, J. Leitz and Q. Zhou, *Annual Review of Biophysics*, 2018, **47**, 469–497.
- 3 C.-W. Chang, C.-W. Chiang and M. B. Jackson, *The Journal of General Physiology*, 2017, **149**, 301–322.
- 4 D. Das, H. Bao, K. C. Courtney, L. Wu and E. R. Chapman, *Nature Communications*, 2020, **11**, 231.
- 5 M. Caparotta, C. N. Tomes, L. S. Mayorga and D. Masone, *J. Chem. Theory Comput.*, 2020, **16**, 7840–7851.
- 6 E. Karatekin, *FEBS letters*, 2018, **592**, 3563–3585.
- 7 A. I. Calejo, J. Jorgacevski, M. Kucka, M. Kreft, P. P. Goncalves, S. S. Stojilkovic and R. Zorec, *The Journal of neuroscience : the official journal of the Society for Neuroscience*, 2013, **33**, 8068–8078.
- 8 K. D. Mackenzie, M. D. Duffield, H. Peiris, L. Phillips, M. P. Zanin, E. H. Teo, X.-F. Zhou and D. J. Keating, *The Journal of physiology*, 2014, **592**, 1505–18.
- 9 A. Gucek, J. Jorgacevski, P. Singh, C. Geisler, M. Lisjak, N. Vardjan, M. Kreft, A. Egner and R. Zorec, *Cellular and molecular life sciences : CMLS*, 2016, **73**, 3719–31.
- 10 C. M. Roggero, G. A. De Blas, H. Dai, C. N. Tomes, J. Rizo and L. S. Mayorga, *Journal of Biological Chemistry*, 2007, **282**, 26335–26343.
- 11 S. Sharma and M. Lindau, *Proceedings of the National Academy of Sciences*, 2018, **115**, 12751–12756.
- 12 H. J. Risselada and H. Grubmüller, *European Biophysics Journal*, 2021, **50**, 279–293.
- 13 P. L. Urban, *New J. Chem.*, 2014, **38**, 5135–5141.
- 14 X. Zhang, X. Shao, Z. Cai, X. Yan and W. Zong, *New J. Chem.*, 2021, **45**, 3364–3376.
- 15 J. M. Dörr, M. C. Koorengevel, M. Schäfer, A. V. Prokofyev, S. Scheidelaar, E. A. W. van der Cruisjen, T. R. Dafforn, M. Baldus and J. A. Killian, *Proc Natl Acad Sci USA*, 2014, **111**, 18607.
- 16 A. R. Long, C. C. O'Brien, K. Malhotra, C. T. Schwall, A. D. Albert, A. Watts and N. N. Alder, *BMC Biotechnology*, 2013, **13**, 41.
- 17 J. M. Dörr, S. Scheidelaar, M. C. Koorengevel, J. J. Dominguez, M. Schäfer, C. A. van Walree and J. A. Killian, *European biophysics journal : EBJ*, 2016, **45**, 3–21.
- 18 C. Tribet, R. Audebert and J.-L. Popot, *Proc Natl Acad Sci USA*, 1996, **93**, 15047.
- 19 N. R. Civjan, T. H. Bayburt, M. A. Schuler and S. G. Sligar, *BioTechniques*, 2003, **35**, 556–563.
- 20 M. Barniol-Xicota and S. H. L. Verhelst, *Communications Biology*, 2021, **4**, 218.
- 21 D. J. K. Swainsbury, S. Scheidelaar, N. Foster, R. van Grondelle, J. A. Killian and M. R. Jones, *Biochimica et Biophysica Acta (BBA) - Biomembranes*, 2017, **1859**, 2133–2143.
- 22 J. M. Dörr, M. H. van Coevorden-Hameete, C. C. Hoogen-

- raad and J. A. Killian, *Biochimica et Biophysica Acta (BBA) - Biomembranes*, 2017, **1859**, 2155–2160.
- 23 A. A. A. Smith, H. E. Autzen, T. Laursen, V. Wu, M. Yen, A. Hall, S. D. Hansen, Y. Cheng and T. Xu, *Biomacromolecules*, 2017, **18**, 3706–3713.
- 24 S. Finkenstaedt-Quinn, S. Gruba and C. Haynes, *Biophysical Journal*, 2016, **110**, 922–929.
- 25 M. P. Zanin, L. Phillips, K. D. Mackenzie and D. J. Keating, *PLoS one*, 2011, **6**, e27820–e27820.
- 26 S. J. Marrink, H. J. Risselada, S. Yefimov, D. P. Tieleman and A. H. de Vries, *J. Phys. Chem. B*, 2007, **111**, 7812–7824.
- 27 P. S. Orekhov, M. E. Bozdoganyan, N. Voskoboynikova, A. Y. Mulkiidjanian, H.-J. Steinhoff and K. V. Shaitan, *Langmuir*, 2019, **35**, 3748–3758.
- 28 C. A. Lopez, Z. Sovova, F. J. van Eerden, A. H. de Vries and S. J. Marrink, *J. Chem. Theory Comput.*, 2013, **9**, 1694–1708.
- 29 H. I. Ingolfsson, M. N. Melo, F. J. van Eerden, C. Arnarez, C. A. Lopez, T. A. Wassenaar, X. Periole, A. H. de Vries, D. P. Tieleman and S. J. Marrink, *J. Am. Chem. Soc.*, 2014, **136**, 14554–14559.
- 30 S. J. Marrink, A. H. de Vries and A. E. Mark, *J. Phys. Chem. B*, 2004, **108**, 750–760.
- 31 A. Perez-Lara, A. Thapa, S. B. Nyenhuis, D. A. Nyenhuis, P. Halder, M. Tietzel, K. Tittmann, D. S. Cafiso and R. Jahn, *eLife*, 2016, **5**, e15886.
- 32 M. Xue, L. Cheng, I. Faustino, W. Guo and S. J. Marrink, *Biophysical journal*, 2018, **115**, 494–502.
- 33 D. Mirjanian, A. N. Dickey, J. H. Hoh, T. B. Woolf and M. J. Stevens, *The journal of physical chemistry. B*, 2010, **114**, 11061–11068.
- 34 S. Qian, W. Wang, L. Yang and H. W. Huang, *Proceedings of the National Academy of Sciences*, 2008, **105**, 17379–17383.
- 35 D. Łoboda, H. Kozłowski and M. Rowińska-Żyrek, *New J. Chem.*, 2018, **42**, 7560–7568.
- 36 M. H. L. Nguyen, M. DiPasquale, B. W. Rikeard, C. G. Yip, K. N. Greco, E. G. Kelley and D. Marquardt, *New J. Chem.*, 2021, **45**, 447–456.
- 37 D. Masone and D. M. Bustos, *Phys. Chem. Chem. Phys.*, 2019, **21**, 268–274.
- 38 M. D'Agostino, H. J. Risselada, L. J. Endter, V. Comte-Miserez and A. Mayer, *The EMBO journal*, 2018, **37**, e99193.
- 39 S. Jo, T. Kim, V. G. Iyer and W. Im, *Journal of Computational Chemistry*, 2008, **29**, 1859–1865.
- 40 S. O. Yesylevskyy, L. V. Schafer, D. Sengupta and S. J. Marrink, *PLOS Computational Biology*, 2010, **6**, 1–17.
- 41 Z. Wu, N. Dharan, Z. A. McDargh, S. Thiyagarajan, B. O'Shaughnessy and E. Karatekin, *bioRxiv*, 2021, 623827.
- 42 Y. G. Smirnova, H. J. Risselada and M. Müller, *Proceedings of the National Academy of Sciences*, 2019, **116**, 2571–2576.
- 43 D. Van Der Spoel, E. Lindahl, B. Hess, G. Groenhof, A. E. Mark and H. J. C. Berendsen, *Journal of Computational Chemistry*, 2005, **26**, 1701–1718.
- 44 S. Pronk, S. Páll, R. Schulz, P. Larsson, P. Bjelkmar, R. Apostolov, M. R. Shirts, J. C. Smith, P. M. Kasson, D. van der Spoel, B. Hess and E. Lindahl, *Bioinformatics*, 2013, **29**, 845–854.
- 45 M. J. Abraham, T. Murtola, R. Schulz, S. Páll, J. C. Smith, B. Hess and E. Lindahl, *SoftwareX*, 2015, **1-2**, 19–25.
- 46 M. Caparotta, D. M. Bustos and D. Masone, *Phys. Chem. Chem. Phys.*, 2020, **22**, 5255–5263.
- 47 D. Masone, M. Uhart and D. M. Bustos, *J. Chem. Theory Comput.*, 2018, **14**, 2240–2245.
- 48 S. Jo, J. B. Lim, J. B. Klauda and W. Im, *Biophysical Journal*, 2009, **97**, 50–58.
- 49 H. Rui, K. I. Lee, R. W. Pastor and W. Im, *Biophysical Journal*, 2011, **100**, 602–610.
- 50 S. Jo, T. Kim and W. Im, *PLoS ONE*, 2007, **2**, e880–.
- 51 G. Bussi, D. Donadio and M. Parrinello, *The Journal of Chemical Physics*, 2007, **126**, 014101.
- 52 H. J. C. Berendsen, J. P. M. Postma, W. F. van Gunsteren, A. DiNola and J. R. Haak, *J. Chem. Phys.*, 1984, **81**, 3684.
- 53 M. Parrinello and A. Rahman, *Journal of Applied Physics*, 1981, **52**, 7182–7190.
- 54 W. Humphrey, A. Dalke and K. Schulten, *Journal of Molecular Graphics*, 1996, **14**, 33–38.